

# Evidence for Evolution Among Primordial Disks in the 5 Myr Old Upper Scorpius OB Association

S. E. Dahm<sup>1,2</sup>

## ABSTRACT

Moderate-resolution, near-infrared spectra between 0.8 and 5.2  $\mu\text{m}$  were obtained for 12 late-type (K0–M3) disk-bearing members of the  $\sim 5$  Myr old Upper Scorpius OB association using SpeX on the NASA Infrared Telescope Facility. For most sources, continuum excess emission first becomes apparent between  $\sim 2.2$  and 4.5  $\mu\text{m}$  and is consistent with that produced by single-temperature blackbodies having characteristic temperatures ranging from  $\sim 500$  to 1300 K. The near-infrared spectra for 5 of 12 Upper Scorpius sources exhibit Pa $\gamma$ , Pa $\beta$  and Br $\gamma$  emission, indicators of disk accretion. Using a correlation between Pa $\beta$  and Br $\gamma$  emission line luminosity and accretion luminosity, mass accretion rates ( $\dot{M}$ ) are derived for these sources that range from  $\dot{M} = 3.5 \times 10^{-10}$  to  $1.5 \times 10^{-8}$   $\text{M}_{\odot} \text{ yr}^{-1}$ . Merging the SpeX observations with *Spitzer Space Telescope* mid-infrared (5.4–37.0  $\mu\text{m}$ ) spectroscopy and 24 and 70  $\mu\text{m}$  broadband photometry, the observed spectral energy distributions are compared with those predicted by two-dimensional, radiative transfer accretion disk models. Of the 9 Upper Scorpius sources examined in this analysis, 3 exhibit spectral energy distributions that are most consistent with models having inner disk radii that substantially exceed their respective dust sublimation radii. The remaining Upper Scorpius members possess spectral energy distributions that either show significant dispersion among predicted inner disk radii or are best described by models having inner disk rims coincident with the dust sublimation radius.

*Subject headings:* clusters: individual (Upper Scorpius OB Association) — stars: pre-main sequence — stars: formation — accretion, accretion disks

---

<sup>1</sup>W. M. Keck Observatory, 65-1120 Mamalahoa Hwy, Kamuela, HI 96743

<sup>2</sup>Visiting Astronomer at the Infrared Telescope Facility, which is operated by the University of Hawaii under Cooperative Agreement no. NNX-08AE38A with the National Aeronautics and Space Administration, Science Mission Directorate, Planetary Astronomy Program.

## 1. Introduction

A fundamental consequence of protostellar collapse is the formation of a viscous accretion disk that transfers gas onto the stellar photosphere. Such disks are the progenitors of planetary systems and their subsequent evolution and ultimate dispersal have extraordinary implications for the formation of planets, orbital dynamics of planetary mass bodies, and the processing of dust grains and volatiles within the disk. The timescale of disk dissipation within the terrestrial region has been reasonably well-established by ground-based (Haisch et al. 2001; Mamajek et al. 2004) and *Spitzer Space Telescope* (Uchida et al. 2004; Silverstone et al. 2006) observations to be  $\leq 10$  Myr. By inference, planetary systems must be in an advanced evolutionary stage within this period, before significant quantities of gas and dust are depleted from the disk. Disk evolution is expected to proceed from the interior outward (Dullemond & Dominik 2005), however, sub-millimeter and mid-infrared observations by Cieza et al. (2008) suggest that inner disks only begin to dissipate after the outer disk has been significantly depleted of mass.

Pre-main sequence stars exhibiting spectral energy distributions (SED) that are indicative of an optically thin disk interior surrounded by an optically thick outer disk are referred to as transition disk objects (Strom et al. 1989; Najita et al. 2007; Muzerolle et al. 2010). Such disks are suggestive of having experienced significant evolution from the continuous disk structures that are associated with classical T Tauri stars (CTTS). The duration of this transitional phase has been inferred from population statistics of star forming regions to be only of order  $\sim 10^5$  yr (Hartmann 2009; Luhman et al. 2010). Transition-like SEDs, however, can arise from various pathways and may not be representative of a direct evolutionary sequence from primordial disk to debris disk (Najita et al. 2007). Dust grain growth and mid-plane settling (Dullemond & Dominik 2005), giant planet formation and dynamical clearing (Calvet et al. 2002), disk photoevaporation (Alexander et al. 2006), and the presence of a stellar companion (Ireland & Kraus 2009) have been suggested as disk clearing mechanisms capable of producing transition-like SEDs. An alternate evolutionary path from primordial disk to debris disk has been proposed by Currie et al. (2009), who suggest that disks exhibiting reduced levels of near- and mid-infrared excess emission are indicative of reduced masses of small dust grains at all disk radii. Such homologously depleted disks counter the canonical inside-out disk evolutionary scenario.

The Upper Scorpius OB association is a critically important region for studies of disk evolution. At  $\sim 145$  pc distant, it is among the nearest OB associations to the Sun (Blaauw 1991; de Zeeuw et al. 1999) and has a well-established age of  $\sim 5$  Myr (Preibisch & Zinnecker 1999; Preibisch et al. 2002), when most ( $\sim 80\%$ ) optically thick, protoplanetary disks have dissipated (Haisch et al. 2001; Hernandez et al. 2007). Carpenter et al. (2006) conducted

a *Spitzer* 4.5–16.0  $\mu\text{m}$  photometric survey of 218 confirmed association members. These sources were compiled from *Hipparcos* astrometry (de Zeeuw et al. 1999), color-magnitude diagrams and Li I  $\lambda 6708$  follow-up observations (Preibisch & Zinnecker 1999; Preibisch et al. 2002), and X-ray detected late-type stars with Li I  $\lambda 6708$  follow-up (Walter et al. 1994; Kunkel 1999; Köhler et al. 2000). Given that the membership selection criteria were based upon stellar properties unrelated to circumstellar material, the sample is considered to be unbiased toward the presence or absence of disks. Carpenter et al. (2006) found that 24 of 127 (19%) K- and M-type stars in their sample exhibit infrared excesses similar to Class II sources in the Taurus-Auriga star forming region. For comparison, Luhman et al. (2010) carried out a comparable *Spitzer* IRAC and MIPS survey of 348 Taurus-Auriga members, finding that the disk fraction steadily declines from  $\sim 75\%$  for solar mass stars to 45% for low-mass stars and brown dwarfs ( $0.3\text{--}0.01 M_{\odot}$ ).

To better characterize disk emission among the Upper Scorpius infrared excess stars identified by Carpenter et al. (2006), Dahm & Carpenter (2009) examined *Spitzer* mid-infrared spectra for a substantial fraction (26 of 35) of these sources: 8 early-type (B+A) stars and 18 late-type (K+M) stars. In general, excess emission among the late-type Upper Scorpius population becomes apparent between 2.2 and 4.5  $\mu\text{m}$ , a region sampled only by Two-Micron All Sky Survey (2MASS)  $K_S$ -band photometry and the *Spitzer* Infrared Array Camera (IRAC) [4.5] fluxes. Compared to Class II sources in Taurus-Auriga, Dahm & Carpenter (2009) found the disk population in Upper Scorpius to exhibit reduced levels of near- and mid-infrared excess emission and an order of magnitude lower mass accretion rates. The apparent abundance of depleted inner disk systems in Upper Scorpius relative to the number of such objects in Taurus-Auriga led Dahm & Carpenter (2009) to suggest that such disks represent a common evolutionary pathway. Near-infrared spectra spanning the 2.2–4.5  $\mu\text{m}$  region, however, were needed to complement the *Spitzer* IRAC and Infrared Spectrograph (IRS) observations and to isolate the onset of continuum excess emission from the terrestrial disk regions.

To further examine emission arising from the depleted disk interiors of the Upper Scorpius sample, 0.8–5.2  $\mu\text{m}$  moderate-resolution spectra for 12 of 18 late-type disk-bearing stars from Dahm & Carpenter (2009) were obtained using SpeX on the NASA Infrared Telescope Facility (IRTF) on Mauna Kea. The SpeX spectroscopy permits the unambiguous detection of continuum excess emission arising from hot dust in the disk interiors of the Upper Scorpius sample. Merging these observations with *Spitzer* IRS spectra and Multi-band Imaging Photometer for *Spitzer* (MIPS) 24 and 70  $\mu\text{m}$  photometry from Carpenter et al. (2009), the resulting 0.8–70  $\mu\text{m}$  SEDs are compared with the two-dimensional, radiative transfer accretion disk models of Robitaille et al. (2006). These models are used to constrain inner disk radii for the observed Upper Scorpius excess sources and to examine their SEDs for

evidence of inner disk evolution.

In Section 2 the observed Upper Scorpius sample is described and placed into context with the greater late-type stellar population of the association. Details of the SpeX observations and analysis are also provided. The near-infrared continuum excess spectra and blackbody fits to these spectra are discussed in Section 3. Next (Section 4) accretion luminosities and mass accretion rates are derived for suspected accretors using  $\text{Pa}\beta$  and  $\text{Br}\gamma$  emission line luminosities. The merged  $0.8\text{--}70\ \mu\text{m}$  SEDs are then compared in Section 5 with the accretion disk models of Robitaille et al. (2006). Constraints for inner disk radii are derived and the effects of mid-plane settling are discussed using the best-fitting accretion disk models. Finally the results of this paper are summarized in Section 6.

## 2. Observations and Analysis

### 2.1. The Upper Scorpius Membership Sample

The 12 Upper Scorpius infrared excess sources observed with SpeX were selected from the mid-infrared photometric and spectroscopic surveys of Carpenter et al. (2006) and Dahm & Carpenter (2009), respectively. These sources represent half of the late-type, disk-bearing stars identified by Carpenter et al. (2006) and include all K-type and all M0 through M2-type excess sources. To further place this sample into context with the low-mass stellar population of Upper Scorpius, there are  $\sim 250$  known pre-main sequence stars in the mass range from  $\sim 0.1$  to  $\sim 2.0\ M_{\odot}$  (Preibisch & Mamajek 2008; Preibisch et al. 2002). If the infrared excess fraction for late-type stars (19%) derived by Carpenter et al. (2006) is assumed,  $\sim 48$  of these should host primordial disks. The SpeX sample therefore represents  $\sim 25\%$  of all disk-bearing stars expected among the known late-type association members. Integrating the best-fitting mass function for Upper Scorpius, Preibisch & Mamajek (2008) estimate that the total low-mass ( $0.1\text{--}2.0\ M_{\odot}$ ) stellar population of the association exceeds 2400 stars, corresponding to a total disk-bearing population of  $\sim 450$  late-type stars. While the SpeX sample considered here does represent a substantial fraction of the late-type, disk-bearing stars identified by Carpenter et al. (2006), it cannot be considered a statistically significant representation of the total low-mass stellar population of the association.

Given that unresolved companions could provide an explanation for transition-like SEDs (Ireland & Kraus 2008), some knowledge of the binary frequency of the Upper Scorpius late-type stellar population is warranted. Köhler et al. (2000) used speckle interferometry and direct imaging for 118 X-ray selected T Tauri stars in the greater Scorpius-Centaurus OB association to identify companions with separations ranging from  $0.13''$  to  $6.0''$ . They found

a multiplicity fraction of  $\sim 32.6\%$ , which exceeds the binary fraction of main sequence stars by a factor  $\sim 1.6$ , but is slightly lower than that observed in Taurus-Auriga (Köhler et al. 2000). Kraus et al. (2008) found a similar frequency of binary companions among 82 late-type (G0–M4) Upper Scorpius members,  $\sim 35 \pm 5\%$ . Two of the disk candidates observed with SpeX are established binaries, [PZ99]J161411.1-230536 and ScoPMS 31, resolved by high angular resolution imaging. With projected separations of  $\sim 32$  and  $84$  AU, respectively (Metchev & Hillenbrand 2009; Köhler et al. 2000), it is unlikely that these stellar companions have significantly influenced the inner disk evolutionary timescales of their primaries. Kraus et al. (2008) observed J160823.2-193001 and J160900.7-190852 using an aperture mask interferometry technique, placing firm upper limits that preclude the possibility of an undetected stellar companion within  $\sim 5$  AU of these stars. The multiplicity fraction among the remaining Upper Scorpius disk-bearing sample is relatively unexplored, but is not expected to deviate significantly from that derived by Köhler et al. (2000) and Kraus et al. (2008) for the pre-main sequence population as a whole.

Shown in Figure 1 is the  $J - H$ ,  $[8.0] - [4.5]$  color-color diagram for the 218 Upper Scorpius members included in the Carpenter et al. (2006) *Spitzer* IRAC and IRS survey. The 12 sources observed with SpeX span the full range of the  $8.0 \mu\text{m}$  excess distribution, from moderate excess (e.g. J160643.8-190805, ScoPMS 31) to significant (e.g. J160900.7-190852). Their masses, derived using the pre-main sequence models of Siess et al. (2000) and assuming a distance of  $145$  pc, range from  $\sim 0.25$  to  $2.0 M_{\odot}$ . General properties of the stellar sample including spectral type, extinction ( $A_V$ ), mass, radius, luminosity, and effective temperature are presented in Table 1.

## 2.2. SpeX Observations

The SpeX (Rayner et al. 2003) observations were made on the nights of 2009 May 20–23 under variable cirrus and seeing conditions ( $0.6$ – $0.9''$ ). The Upper Scorpius members were observed in the short cross-dispersed SXD ( $0.84$ – $2.4 \mu\text{m}$ ) and long cross-dispersed LXD ( $2.2$ – $5.2 \mu\text{m}$ ) modes for complete near-infrared wavelength coverage. Bright A0 V stars were observed at similar airmasses ( $\Delta\chi < 0.1$ ) and within short periods of time of the program stars for telluric correction. Arc-lamps and internal flat-field exposures were obtained for each set of observations to account for instrument flexure. All observations were made with the  $0.5''$  slit yielding a nominal spectral resolution of  $\lambda/\delta\lambda \sim 1500$ .

The spectra were reduced using *Spextool*, an IDL-based reduction package that provides for sky-subtraction, flat-fielding, wavelength calibration, and optimal extraction (Cushing et al. 2004). For telluric corrections *xtellcor*, an extension package of *Spextool*, was used

to create a kernel for the telluric spectrum using a model spectrum of  $\alpha$  Lyra. *xtellcor* interpolates over broad hydrogen absorption lines in the spectra of the A0 V stars using a technique developed by Vacca et al. (2003). The orders of the telluric corrected spectra were then combined and the SXD and LXD spectra merged using routines available within *Spextool*. The resulting continuum levels across all orders and between the SXD and LXD modes were found to be remarkably consistent. The near infrared spectra were then merged with the *Spitzer* IRS spectra. Details of the *Spitzer* IRS observations and their subsequent reduction and analysis can be found in Dahm & Carpenter (2009).

### 3. Near-Infrared Continuum Excess Spectra

The extinction-corrected, near-infrared ( $0.84\text{--}5.2\ \mu\text{m}$ ) spectra of the 12 Upper Scorpius sources are shown in Figure 2. Regions of strong telluric absorption (atmospheric transmission  $<20\%$ ) have been excised from the figure. Also shown are the spectra of solar metallicity, main sequence stars of identical or closely matched ( $\pm 1$  sub-class) spectral type obtained from the IRTF spectral library (Rayner et al. 2009). These standards have reliable spectral types and are directly linked to the MK classification system. The standard or template spectra are scaled to the flux levels of the Upper Scorpius sources at  $1.65\ \mu\text{m}$ , near the peak of the stellar SED and where extinction effects are minimized (D’Alessio et al. 1999; Furlan et al. 2006).

To characterize excess emission attributable to the inner disk rim, the scaled photospheric template spectra are subtracted from the dereddened spectra of the Upper Scorpius sample. The resulting continuum excess spectra are shown in Figure 3. Significant noise is present due to imperfect telluric correction, particularly in the thermal region where the water column varies both temporally and with airmass. In general, the slopes of the continuum excess spectra are increasing from  $K$ -band to  $\sim 3.5\ \mu\text{m}$  before turning over toward redder wavelengths. The shapes of many of the continuum excess spectra are suggestive of having been produced by single-temperature blackbodies. By fitting these excess spectra with Planck functions, the characteristic temperatures of the blackbodies are found to range from the sublimation temperature for silicate dust, i.e.  $\sim 1400\ \text{K}$ , to  $\leq 500\ \text{K}$ . The slope of excess emission, particularly between  $\sim 2.75$  and  $4.2\ \mu\text{m}$ , was found to be of critical importance when fitting the blackbody profiles to the continuum excess spectra.

To estimate the uncertainty associated with the derived blackbody temperatures, photospheric templates within a range of  $\pm 1$  sub-class of the assigned spectral type were subtracted from the Upper Scorpius spectra. The best-fitting blackbody curves for this range of photosphere-subtracted excess spectra suggest typical uncertainties of  $\sim \pm 200\ \text{K}$  for most

sources. The adopted blackbody curve as well as curves representing the limits of uncertainty in the characteristic temperature are shown in Figure 3. The characteristic temperatures of the best-fitting blackbodies are provided in Table 1 and are assumed to be representative of the dust temperatures in the disk interiors.

The disk fractions of Upper Scorpius and Taurus-Auriga differ significantly for the range in stellar masses considered here: 19% for the former (Carpenter et al. 2006) and up to 75% for the latter (Luhman et al. 2010). Muzerolle et al. (2003) used SpeX in LXD-mode to observe 9 CTTSs in Taurus-Auriga, 8 of which span a range of spectral types (G5–M1), luminosities ( $12.8\text{--}0.5\ L_{\odot}$ ), and stellar radii ( $3.6\text{--}1.8\ R_{\odot}$ ) that are comparable with those of the Upper Scorpius disk sample. Restricting further comparison of these samples to just those sources having similar physical properties (i.e. spectral type, luminosity), the spectral profiles of continuum excess emission of the Upper Scorpius disks are found to differ from those of Class II sources in Taurus-Auriga. For 6 of 9 members in the reduced Upper Scorpius sample, the characteristic temperatures of excess emission fall below the dust sublimation temperature, a condition satisfied by only one member (the binary DQ Tau) of the Taurus-Auriga sample. Furthermore, the excess profiles of J160643.8-190805 and J160357.9-194210, which are not represented in Figure 3, exhibit no distinctive shape, implying minimal continuum excess emission at near-infrared wavelengths. Shallow rises may be present near  $\sim 3.75\ \mu\text{m}$  for these 2 sources, suggestive of warm ( $\leq 500\ \text{K}$ ) dust emission, but higher SN spectra are needed for confirmation. The excess spectra of J161420.2-190648, [PZ99]J160357.6-203105, J160900.7-190852, and J155829.8-231007 all have characteristic temperatures at or near the dust sublimation temperature, implying that emission arises from dust in close proximity to the host star. Of these sources, all are suspected accretors (Section 4).

#### 4. Accretion Luminosity and Mass Accretion Rates

Dahm & Carpenter (2009) identified 5 Upper Scorpius members in the present sample as probable accretors using the  $\text{H}\alpha$  velocity width criteria of White & Basri (2003): [PZ99]J160357.6-203105 (K5), J160900.7-190852 (K7), J161420.2-190648 (M0), ScoPMS 31 (M0.5), and J155829.8-231007 (M3). The near-infrared spectra of these sources exhibit He I  $\lambda 10830$ ,  $\text{Pa}\gamma$ , and  $\text{Pa}\beta$  emission and for most, weak  $\text{Br}\gamma$  emission. Shown in Figure 4 are the normalized spectra of these sources centered upon  $\text{Pa}\gamma$ ,  $\text{Pa}\beta$ , and  $\text{Br}\gamma$ . Dahm & Carpenter (2009) used veiling at  $\lambda 6500\ \text{\AA}$  as well as Ca II  $\lambda 8542$  emission line luminosity to estimate mass accretion rates ( $\dot{M}$ ) for these stars. In the near-infrared, Muzerolle et al. (1998) found  $\text{Pa}\beta$  and  $\text{Br}\gamma$  emission line luminosity ( $L_{\text{Pa}\beta}$  and  $L_{\text{Br}\gamma}$ ) to be well-correlated with accretion luminosity,  $L_{\text{acc}}$ . The resulting least-squares fits from Muzerolle et al. (1998) are given by:

$$\log\left(\frac{L_{acc}}{L_{\odot}}\right) = (1.14 \pm 0.16)\log\left(\frac{L_{Pa\beta}}{L_{\odot}}\right) + 3.15 \pm 0.58 \quad (1)$$

and

$$\log\left(\frac{L_{acc}}{L_{\odot}}\right) = (1.26 \pm 0.19)\log\left(\frac{L_{Br\gamma}}{L_{\odot}}\right) + 4.43 \pm 0.79 \quad (2).$$

For the 5 suspected accretors in the Upper Scorpius sample, template spectra of identical or similar spectral type from the IRTF spectral library of Rayner et al. (2009) were used to subtract  $Pa\beta$  and  $Br\gamma$  photospheric absorption.  $Pa\beta$  and  $Br\gamma$  line luminosities were then determined using their measured equivalent widths and the extinction-corrected  $J$ – and  $K_S$ –band magnitudes obtained from the 2MASS point source catalog. The resulting emission line luminosities were then transformed into  $L_{acc}$  using the above linear relationships of Muzerolle et al. (1998). The derived  $L_{acc}$  values are directly proportional to  $\dot{M}$  such that:

$$L_{acc} \sim \frac{GM_*\dot{M}}{R_*}(1 - \frac{R_*}{R_{in}}) \quad (3)$$

where the stellar mass and radius estimates used are those predicted by the pre-main sequence models of Siess et al. (2000). The factor of  $(1 - R_*/R_{in})$  is assigned a value of 0.8, which assumes an inner disk radius ( $R_{in}$ ) of  $5 R_*$  (Gullbring et al. 1998). Given the possibility that inner disk radii for the Upper Scorpius sources may exceed those of typical Class II sources in Taurus-Auriga, this value could be underestimated by a factor of  $\sim 1.25$ . The derived  $L_{acc}$  and  $\dot{M}$  values with their associated uncertainties are presented in Table 2. These uncertainties arise from multiple sources: error in the measured equivalent width (assumed to be  $\sim 20\%$ ), spectral type uncertainty when correcting for photospheric absorption ( $\pm 1$  sub-class), the uncertainty in each coefficient of the Muzerolle et al. (1998) relationships, and the uncertainty in  $R_{in}$  when determining  $\dot{M}$  values.

In general the  $\dot{M}$  values derived using  $L_{Pa\beta}$  and  $L_{Br\gamma}$  agree reasonably well with each other and with the  $\dot{M}$  values from the veiling and Ca II  $\lambda 8542$  analysis of Dahm & Carpenter (2009). In summary, 5 of 12 of the Upper Scorpius sample are accreting, providing unambiguous evidence for the presence of gas within the terrestrial regions of these disk-bearing systems.

## 5. Accretion Disk Model Analysis

To further examine inner disk structure and to constrain inner disk radii for the Upper Scorpius disk-bearing sample, the observed SEDs are compared with those predicted by the accretion disk models of Robitaille et al. (2006). To facilitate the comparison, the flux-calibrated SpeX observations presented here are merged with the *Spitzer* IRS low-resolution spectra and MIPS 24 and 70  $\mu\text{m}$  fluxes taken from Dahm & Carpenter (2009) and Carpenter



et al. (2009), respectively. The resulting 0.8–70  $\mu\text{m}$  SEDs are well sampled between 2.2 and 24  $\mu\text{m}$ , a spectral region dominated by disk emission originating from the terrestrial region.

The Robitaille et al. (2006) grid of pre-computed, two-dimensional radiative transfer models consists of 20,000 young stellar objects in varying stages of evolution and viewed from 10 inclination angles. A total of 14 parameters are randomly sampled that specify stellar (e.g.  $M_*$ ,  $R_*$ ,  $T_{eff}$ ) as well as disk (e.g.  $M_{disk}$ ,  $\dot{M}$ ,  $R_{min}$ ) properties. The models have been successfully applied to the SEDs of 30 spatially resolved Class I and II sources in Taurus-Auriga by Robitaille et al. (2007), including the transition disk objects GM Aur and DM Tau.

The SEDs of 9 Upper Scorpius members were compared to the accretion disk models. The sources excluded from the model fitting analysis were J160545.4-202308 and J155829.8-231007, which were not observed with IRS, and [PZ99]J160421.7-213028, which exhibited significant (factor of  $\sim 4$ ) mid-infrared variability (Dahm & Carpenter 2009). To compare the observed SEDs with the accretion disk models, fluxes were measured in  $\sim 30$  narrow passbands defined between 0.8 and 37.0  $\mu\text{m}$ . The MIPS 24 and 70  $\mu\text{m}$  fluxes were also incorporated, with the 70  $\mu\text{m}$  fluxes being used to constrain disk emission originating from beyond the terrestrial region.

Two assumptions were made in the model fitting analysis: that all Upper Scorpius members lie between 125 and 185 pc distant, and that foreground extinction is no more than  $A_V \sim 3$  mag, both reasonable assumptions based upon substantial Upper Scorpius literature (e.g. Preibisch & Zinnecker 1999; Preibisch et al. 2002; Carpenter et al. 2006). A range of effective temperatures was defined for each Upper Scorpius source based upon its adopted spectral type and assuming an uncertainty of  $\pm 1$  spectral sub-class. Only models having effective temperatures within this specified range were considered when fitting the observed SEDs. The model fitting program was written in IDL and uses the  $\chi^2$  statistic to evaluate the goodness of fit of each model for each assumed distance, extinction value, and inclination angle. Table 3 lists the range of  $T_{eff}$  values considered for each Upper Scorpius source, the number of models included within the specified range, the best-fitting model number, its corresponding  $A_V$ , distance, and inclination angle, and the minimum reduced  $\chi^2$  value achieved by the fit.

Shown in the upper panels of Figures 5a–i are the observed 0.8–70.0  $\mu\text{m}$  SEDs for the 9 Upper Scorpius sources included in the model fitting analysis. Superimposed in red are the best-fitting model profiles placed at their respective distances and extinctions. The disk contributions to the model SEDs are represented by the dotted black curves, and the model stellar atmospheres, taken from the Kurucz (1979) atlas, are plotted in blue. In general, reasonable fits were achieved for many of the Upper Scorpius disk-bearing stars

despite the modest number of models (typically  $\leq 2000$ ) examined for each source. The near-infrared spectrum of the strongly accreting source J161420.2-190648 is suggestive of significant extinction,  $A_V \sim 6$  mag, (Figure 5f). The optimal model fits for this source yielded the largest  $\chi^2$  values of the sample given the a priori assumption that  $A_V \leq 3$  mag.

Degeneracy among model SEDs having significantly different stellar and disk properties is an inherent limitation of the SED fitting process. It is possible, however, to place constraints upon a specific parameter by examining the range of values returned by the best-fitting models. To identify this subset of models,  $\chi^2 - \chi_{min}^2 < N$  is used as a statistical measure of goodness of fit, where  $\chi_{min}^2$  is the minimum  $\chi^2$  value returned by the fitting process and  $N$  is set to the  $1-\sigma$  confidence interval for  $\nu$  degrees of freedom. In Table 4 the disk properties of the Upper Scorpius sample obtained from these best-fitting subsets are summarized. Tabulated for each source are the minimum, best-fitting, and maximum values of disk mass ( $M_{disk}$ ),  $\dot{M}$ , and inner disk radius ( $R_{in}$ ). The ranges of  $M_{disk}$  and  $\dot{M}$  are significant, up to several orders of magnitude separating the minimum and maximum values for a given source. The observed dispersion in  $M_{disk}$  arises in part from the lack of far-infrared or millimeter wavelength observations that could constrain outer disk emission where substantial quantities of disk mass could remain unaccounted for. Mass accretion rates calculated by the models were found by Robitaille et al. (2007) to be overestimated in their sample of Taurus sources. In the Upper Scorpius sample, whether established accretors or not,  $\dot{M}$  is observed to range at least 3 orders of magnitude, and in some cases up to 5. For most suspected accretors included in the model fitting analysis, the  $\dot{M}$  values derived in Section 4 using the Pa $\beta$  and Br $\gamma$  emission line luminosities are consistent with those predicted by the best-fitting models.

As might be expected, inner disk radius appears to be better constrained by the subsets of best-fitting models than either  $M_{disk}$  or  $\dot{M}$ . Several Upper Scorpius sources, e.g. [PZ99]J161411.0-230536, [PZ99]J160357.6-203105, and ScoPMS 31, exhibit ranges in  $R_{in}$  from minimum to maximum of an order of magnitude or less. Five sources have best-fitting inner disk radii that exceed their respective dust sublimation radii: [PZ99]J161411.0-230536 ( $R_{in}=0.87$  AU), J160900.7-190852 (2.18 AU), ScoPMS 31 (9.62 AU), J161115.3-175721 (0.29 AU), and J160357.9-194210 (0.17 AU). Given the poor quality of the  $\chi^2$  fit for the strongly accreting source J161420.2-190648, the best-fitting  $R_{in}$  value of 0.8 AU is regarded with skepticism. The remaining Upper Scorpius sources ([PZ99]J160357.6-203105, J160643.8-190805, and J160823.2-193001) have best-fitting inner disk radii that are consistent with their sublimation radii. The confidence levels for these inner disk radii, however, are best examined in terms of a probability density function determined from the  $\chi^2$  values of the accretion disk model fits.

### 5.1. Constraints for Inner Disk Radii

Flux from the terrestrial disk regions is well sampled by the SpeX and IRS observations, which are dominated by disk emission extending from the sublimation radius to more than 20 AU for a typical  $\sim 0.7 M_{\odot}$  pre-main sequence star. The Upper Scorpius disks are presumably at an advanced evolutionary stage relative to those found around Class II sources in Taurus-Auriga and exhibit SEDs that are consistent with reduced levels of near and mid-infrared disk emission (Dahm & Carpenter 2009). Robitaille et al. (2007) find that all Taurus sources, except for the known transition disk objects (e.g. GM Aur, DM Tau) can be fit by models having disks and envelopes with inner disk radii equal to the dust sublimation limit. Approximately one-third of the Robitaille et al. (2006) models have inner disk radii set to the dust destruction radius. The remaining models have increasing inner disk radii that span from the dust destruction radius to 100 AU. The inner disk gaps are treated by the models as being completely evacuated of dust (Robitaille et al. 2006).

To constrain  $R_{in}$  for the Upper Scorpius disk sample a probability ( $P$ ) is calculated for a given inner disk radius using the returned  $\chi^2$  values from the model fits of the observed SEDs:

$$P = \frac{1}{\sqrt{2\pi}} e^{-\frac{\chi^2}{2}} \quad (4)$$

This probability density function assumes a normal distribution for the returned  $\chi^2$  values of the individual fits. In the center panels of Figures 5a–i,  $P$  is plotted as a function of  $R_{in}$  for each Upper Scorpius source. Superimposed in the figures as cross-hatched histograms are the distributions of inner disk radii for the entire sample of models considered for each source. Only 3 Upper Scorpius disks have predicted inner radii that are larger than their respective dust sublimation radii at the  $1\sigma$  confidence level or greater: [PZ99]J161411.0-230536 ( $2\sigma$ ), J160900.7-190852 ( $1\sigma$ ), and ScoPMS31 ( $3\sigma$ ). The remaining sources have inner disk radii that are either most consistent with the sublimation radius or exhibit a broad dispersion among predicted  $R_{in}$  values (e.g. J161115.3-175721). The SED of J160643.8-190805, which exhibits minimal near-infrared continuum excess emission (Section 3), is readily fit by a large number of models having a range of inner disk radii. This source exhibits an SED that is reminiscent of those defined as anemic (Lada et al. 2006), weak (Dahm & Hillenbrand 2007), or homologously depleted disk-bearing systems (Currie et al. (2009).

### 5.2. Disk Mid-plane Settling

The current disk evolution scenario suggests that dust grains coagulate and settle toward the mid-plane prior to the formation of large planetesimals. The Robitaille et al. (2006)

models use 2 disk structure parameters to mimic the effects of dust settling: a disk flaring parameter ( $\beta$ ) and a disk scale height factor ( $z$ ). If both of these parameters are low for a given model, this could be indicative of dust mid-plane settling (Robitaille et al. 2006). In the lower panels of Figures 5a–i  $\beta$  is plotted as a function of  $z$  for the entire sample of models considered for each source. Superimposed in red are the best-fitting models as determined by the  $\chi^2 - \chi_{min}^2 < N$  measure of goodness of fit. In general the spread in both parameters for the best-fitting models is significant, suggesting that neither is well-constrained. Some argument can be made that the SEDs of [PZ99]J161411.0-230536, J160643.8-190805, and ScoPMS31 are better fit by models having lower than average values of  $\beta$ . The disk scale height factors for these sources, however, are found to vary significantly. Evidence for dust settling effects among the Upper Scorpius primordial disk sample remains inconclusive at best.

## 6. Discussion and Conclusions

The clearly different near- and mid-infrared color excess distributions of the Upper Scorpius and Taurus-Auriga Class II populations found by Dahm & Carpenter (2009) suggest that the Upper Scorpius stars have experienced some degree of inner disk evolution relative to their presumably younger counterparts in Taurus-Auriga. This is circumstantially supported by the characteristic temperatures of the continuum excess emission for most Upper Scorpius sources, which are substantially lower than the sublimation temperature for silicate dust. This condition is satisfied by only one member of the Muzerolle et al. (2003) Taurus-Auriga sample of Class II sources having similar spectral types and luminosities. The accretion disk model fitting results, however, are unable to effectively constrain inner disk radii for the majority of the Upper Scorpius disk-bearing sample. This could in part result from the limited number of models examined for each source, which do not sample the full range of available parameter space of disk structure. Another limitation of the Robitaille et al. (2006) models is the assumption that disk gaps are completely devoid of dust, a reduction in complexity that impacts the predicted near- and mid-infrared excess distributions, critical for constraining disk emission originating from the inner disk rim.

In summary 3 of 9 late-type, disk-bearing stars in the Upper Scorpius sample exhibit SEDs that are most consistent with having inner disk radii that lie beyond the sublimation radius for silicate dust: [PZ99]J161411.0-230536, J160900.7-190852, and ScoPMS31. The best-fitting models for 2 additional sources: J161115.3-175721 and J160357.9-194210, have inner disk radii that substantially exceed their respective dust sublimation radii, but the probability distributions of  $R_{in}$  values for these sources exhibit significant dispersion. Pro-

posed indicators for the effects of mid-plane settling in the best-fitting Robitaille et al. (2007) models of the Upper Scorpius sample (i.e. concurrent decreased values of the disk flaring parameter and disk scale height factor) are inconclusive, leaving open to question the nature of the remaining Upper Scorpius primordial disks and their evolutionary state.

Transition disks are believed to represent an early stage of disk clearing and may be in the process of rapid grain growth, planetesimal and planet formation. Adopting the disk classification scheme of Luhman et al. (2010), many Upper Scorpius sources would be classified as pre-transitional objects, i.e. disks that exhibit reduced emission at wavelengths  $\leq 10 \mu\text{m}$ , but that still retain significant disk emission at longer wavelengths. Two of the Upper Scorpius pre-transitional candidates appear to exhibit gapped disk structure: J160900.7-190852 and ScoPMS31. Both sources are accreting (Dahm & Carpenter 2009 and Section 4) and both exhibit SEDs that are most consistent with having substantial inner disk radii,  $\sim 1\text{--}10$  AU. At least one Upper Scorpius source, J160643.8-190805, exhibits an infrared SED that is suggestive of an homologously depleted disk system as defined by Currie et al. (2009).

Before attributing the reduced levels of infrared excess emission in the Upper Scorpius sample to disk evolutionary processes, binarity must be considered as an explanation for the cleared out inner cavities (e.g. CoKu Tau 4, Ireland & Kraus 2008). Two of the disk candidates included in this analysis, [PZ99]J161411.1-230536 and ScoPMS 31, are established binaries resolved by high angular resolution imaging. It must also be acknowledged that the SpeX sample represents only  $\sim 25\%$  of all primordial disk-bearing stars expected among the  $\sim 250$  known late-type members of the Upper Scorpius OB association. Observations of more late-type, disk-bearing systems are critically needed to confirm the results presented here.

Improved modeling of the Upper Scorpius primordial disk-bearing sample is clearly needed to provide better constraints for the inner disk structure of these presumably evolved primordial disk systems. Monte Carlo three-dimensional, radiative transfer codes are now available that could be applied to the SEDs of these sources. High angular resolution imaging is also needed to identify close ( $\leq 10$  AU) binary companions that may account for the reduced near- and mid-infrared excess emission of these sources relative to Class II sources in Taurus-Auriga. Infrared interferometric observations or precision radial velocity monitoring are also needed to identify tighter pairs or spectroscopic binaries that would be capable of dynamically clearing the disk interiors of these systems.

This work is based on observations made with the *Spitzer* Space Telescope, which is operated by the Jet Propulsion Laboratory (JPL), California Institute of Technology, under NASA contract 1407. The Digitized Sky Surveys, which were produced at the Space Telescope Science Institute under U.S. Government grant NAG W-2166, were used as were the

the SIMBAD database operated at CDS, Strasbourg, France, and the Two Micron All Sky Survey (2MASS), a joint project of the University of Massachusetts and the Infrared Processing and Analysis Center (IPAC)/California Institute of Technology, funded by NASA and the National Science Foundation. The author gratefully acknowledges John Carpenter and an anonymous referee for many helpful suggestions that significantly improved this manuscript. The author also thanks Elise Furlan, Thayne Currie, and Joan Najita for insightful discussions and Thomas Robitaille for graciously providing direct access to the accretion disk models. Finally the author thanks John Rayner for obtaining a second-epoch SpeX SXD spectrum of [PZ99]J160421.7-213028.

## REFERENCES

- Alexander, R. D., Clarke, C. J., & Pringle, J. E. 2006, *MNRAS*, 369, 229
- Blaauw, A. 1991, in *The Physics of Star Formation and Early Stellar Evolution*, ed. C. J. Lada & N. D. Kylafis (Dordrecht: Kluwer), 125
- Calvet, N. et al. 2002, *ApJ*, 568, 1008
- Carpenter, J. M., Mamajek, E. E., Hillenbrand, L. A., & Meyer, M. R. 2006, *ApJ*, 651, L49
- Carpenter, J. M., Mamajek, E. E., Hillenbrand, L. A., & Meyer, M. R. 2009, *ApJ*, 705, 1646
- Cieza, L. A., et al. 2008, *ApJL*, 686, 115
- Currie, T., Lada, C. J., Plavchan, P., Robitaille, T. P., Irwin, J. et al. *ApJ*, 698, 1
- Cushing, M. C., Vacca, W. D., & Rayner, J. T. 2004, *PASP*, 116, 362
- Dahm, S. E. & Carpenter, J. M. 2009, *AJ*, 137, 4024
- Dahm, S. E. & Hillenbrand L. A. 2007, *AJ*, 133, 2072
- D’Alessio, P., Canto, J., Hartmann, L., Calvet, N., & Lizano, S. 1999, *ApJ*, 511, 896
- de Zeeuw, P. T., Hoogerwerf, R., de Bruijne, J. H. J., Brown, A. G. A., & Blaauw, A. 1999, *AJ*, 117, 354
- Dullemond, C. P. & Dominik, C. 2005, *A&A*, 434, 971
- Furlan, E. et al. 2006, *ApJS*, 165, 568
- Gullbring, E., Hartmann, L., Briceno, C. 1998, *ApJ*, 492, 323
- Haisch, K. E., Jr., Lada, E. A., & Lada, C. J. 2001, *ApJ*, 553, L153
- Hartmann, L. 2009, in *Accretion Processes in Star Formation: Second Edition*, Cambridge University Press, Cambridge, UK

- Hernandez, J. et al. 2007, ApJ, 671, 1784
- Ireland, M. J. & Kraus, A. 2008, ApJ, 678, 59L
- Köhler, R., Kunkel, M., Leinert, C., & Zinnecker, H. 2000, A&A, 356, 541
- Kraus, A. L., Ireland, M. J., Martinache, F., & Lloyd, J. P. 2008, ApJ, 679, 762
- Kurucz, R. L. 1979, ApJSS, 40, 1
- Lada, C. J. et al. 2006, 131, 1574
- Luhman et al. 2010, ApJS, 186, 111
- Mamajek, E. E., Meyer, M. R., Hinz, P. M., Hoffmann, W. F., Cohen, M., & Hora, J. L. 2004, ApJ, 612, 496
- Muzerolle, J., Hartmann, L., & Calvet, N. 1998, AJ, 116, 2965
- Muzerolle, J., Calvet, N., Hartmann, L., & D'Alessio, P. 2003, ApJ, 597, 149
- Muzerolle, J., Allen, L. E., Megeath, S. T., Hernandez, J., & Gutermuth, R. A. 2010, ApJ, 708, 1107
- Metchev, S. & Hillenbrand, L. A. 2009, ApJS, 181, 62
- Najita, J. R., Strom, S. E., & Muzerolle, J. 2007, MNRAS, 378, 369
- Preibisch, T., & Zinnecker, H. 1999, AJ, 117, 2381
- Preibisch, T., Brown, A. G. A., Bridges, T., Guenther, E., & Zinnecker, H. 2002, AJ, 124, 404
- Preibisch, T. & Mamajek, E. 2008, in The Handbook of Star Forming Regions Vol. II, ed. B. Reipurth (ASP), 235
- Rayner, J. T. et al. 2003, PASP, 115, 362
- Rayner, J. T., Cushing, M. C., & Vacca, W. D. 2009, ApJS, 185, 289
- Robitaille, T. P., Whitney, B. A., Indebetouw, R., & Wood, K. 2007, ApJS, 169, 328
- Robitaille, T. P., Whitney, B. A., Indebetouw, R., Wood, K., & Denzmore, P. 2006, ApJS, 167, 256
- Siess, L., Dufour, E., & Forestini, M. 2000, A&A, 358, 593
- Silverstone, M. D., Meyer, M. R., Mamajek, E. E., Hines, D. C., Hillenbrand, L. A., Najita, J. et al. 2006, ApJ, 639, 1138
- Strom, K. M. et al. 1989, AJ, 97, 1451
- Uchida, K. I., Calvet, N., Hartmann, L., Kemper, F., Forrest, W. J. et al. 2004, ApJS, 154, 539

- Vacca, W. D., Cushing, M. C., & Rayner, J. T. 2003, *PASP*, 115, 389
- White, R. J. & Basri, G. 2003, *ApJ*, 582, 1109



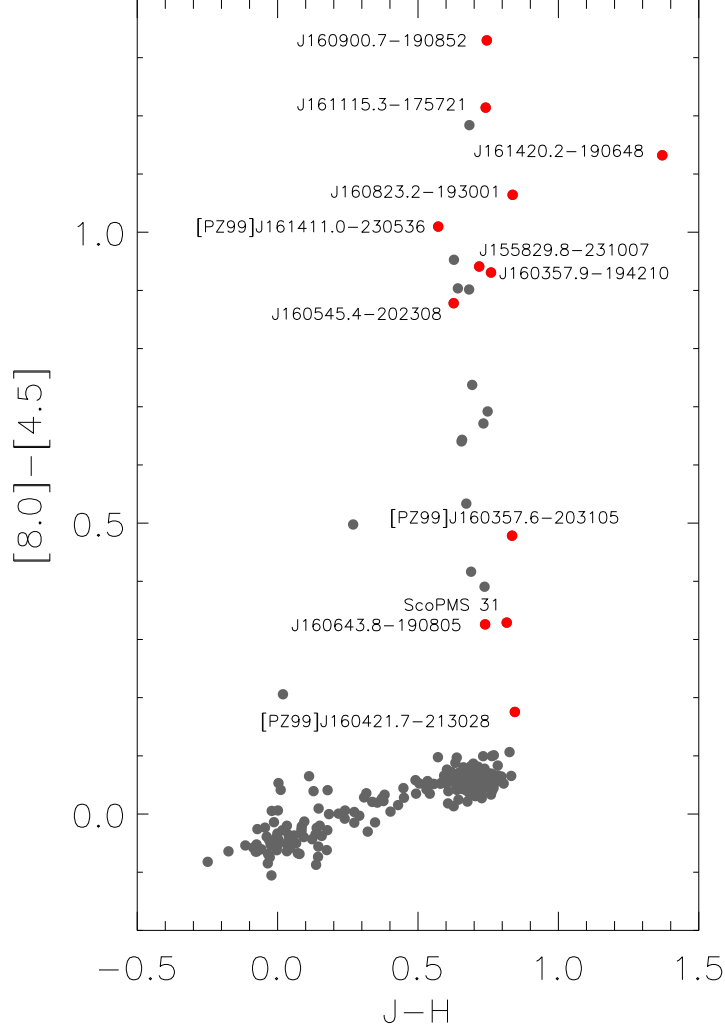


Fig. 1.— The  $J - H$ ,  $[8.0] - [4.5]$  color-color diagram for 218 Upper Scorpius members from the *Spitzer* IRAC and IRS survey of Carpenter et al. (2006). Shown in red are the 12 late-type disk-bearing stars observed with SpeX. The sources span the full range of the 8.0  $\mu\text{m}$  excess distribution, from slight excess (e.g. J160643.8-190805, ScoPMS 31) to significant (e.g. J160900.7-190852).

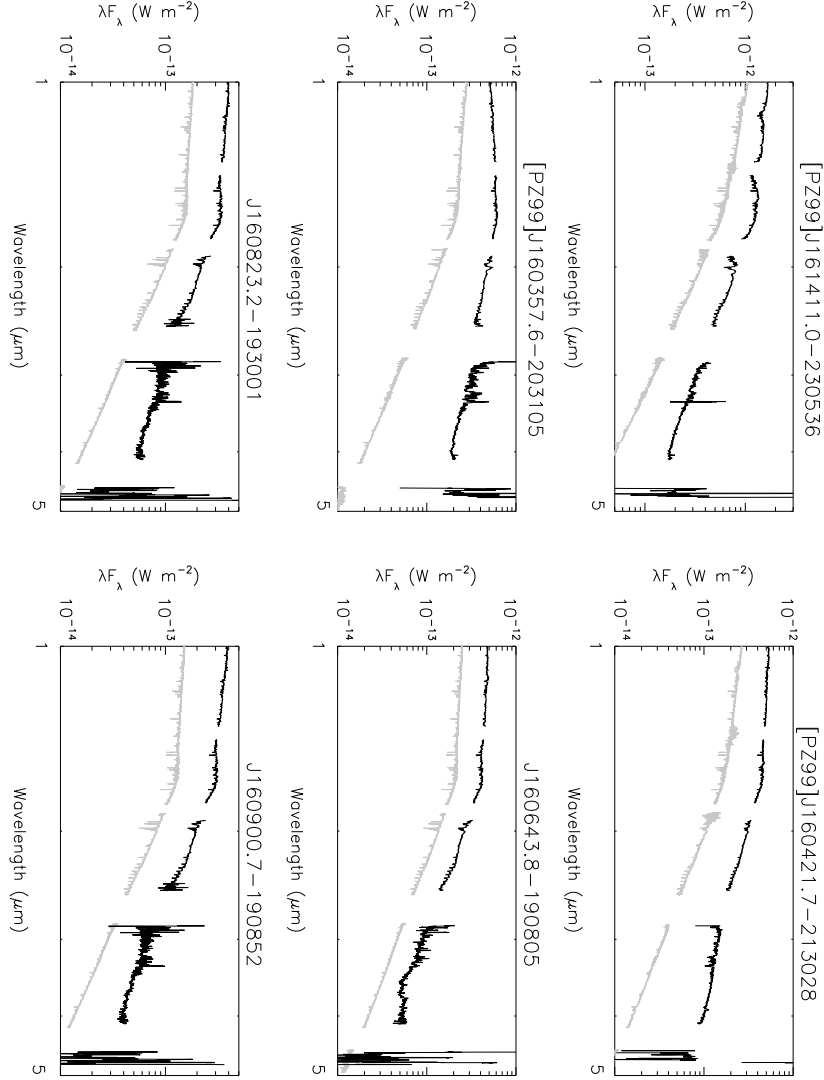


Fig. 2.— The SpeX near infrared (0.84–5.2  $\mu\text{m}$ ) spectra of the 12 late-type disk-bearing stars in Upper Scorpius, de-reddened by their individual extinctions tabulated in Dahm & Carpenter (2009). Superimposed in gray are the spectra of solar metallicity, main sequence stars of identical spectral type or closely matched obtained from the IRTF spectral library (Rayner et al. 2009). The standard spectra are scaled to the flux levels of the Upper Scorpius sources near 1.65  $\mu\text{m}$ , where stellar photospheric flux peaks and where extinction effects are minimized. For the purpose of display, the standard spectra are offset from the object spectra by an additive constant.

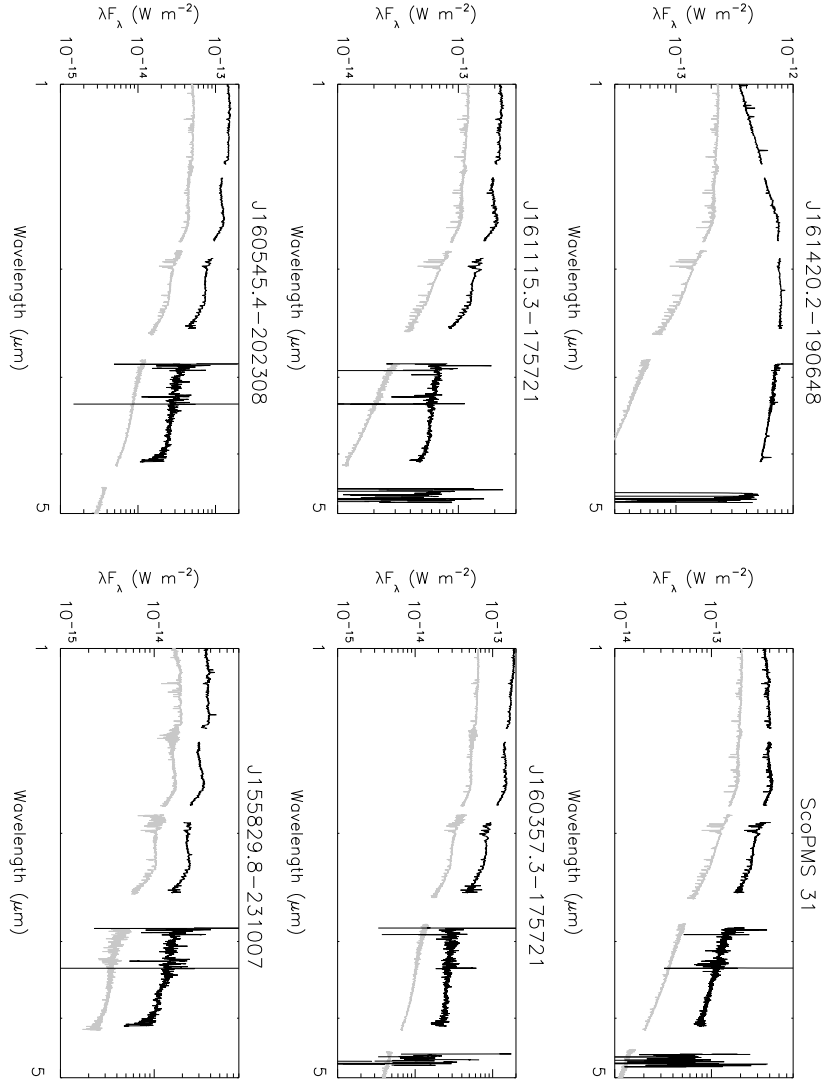


Fig. 2.— (continued)

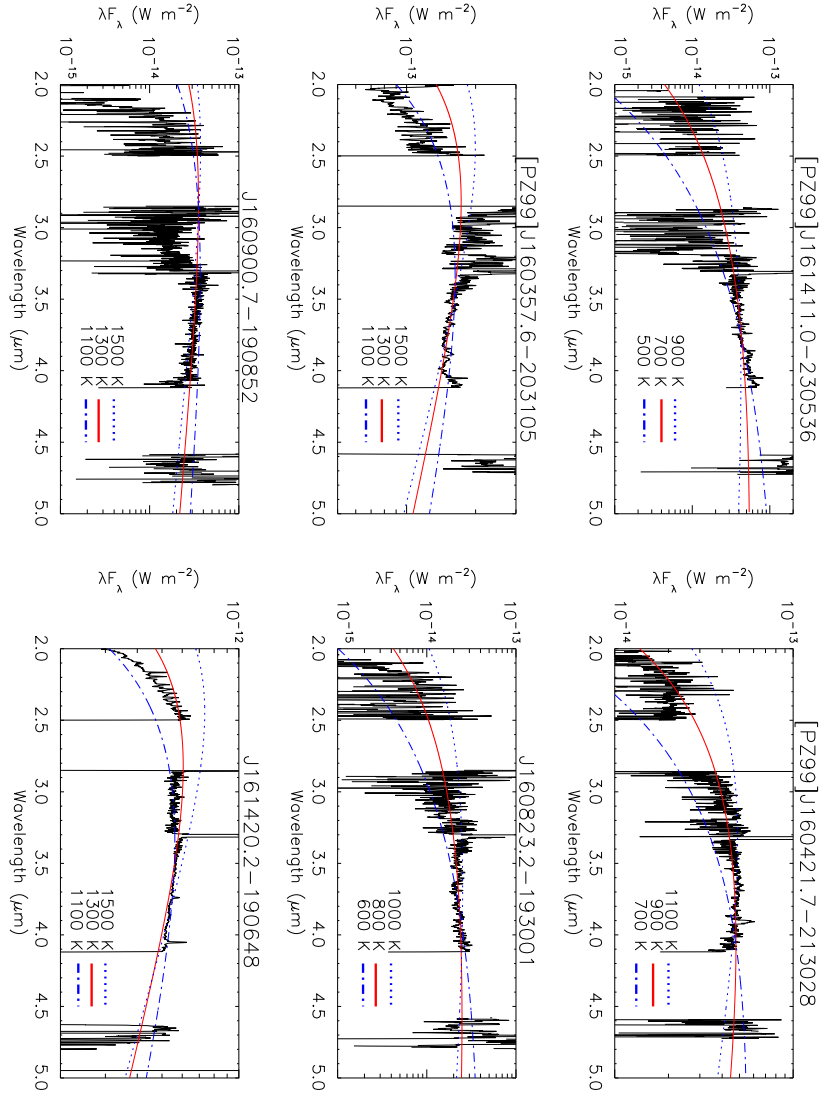


Fig. 3.— The near-infrared continuum excess spectra for 10 Upper Scorpius late-type, disk-bearing stars created by subtracting scaled photospheric template spectra obtained from the IRTF spectral library (Rayner et al. 2009) from the dereddened object spectra. The template spectra are of identical spectral type of the Upper Scorpius sources or closely matched, within  $\pm 1$  subclass. Significant noise is present due to imperfect telluric correction, particularly in the thermal region where the water column varies both temporally and with airmass. Shown in red are the Planck functions that best fit the continuum excess spectra. Most have characteristic temperatures ranging from the dust sublimation temperature, near  $\sim 1400$  K, to less than  $\sim 500$  K. Also depicted (in blue) are blackbody curves representing the upper and lower limits of uncertainty associated with the blackbody characteristic temperatures.

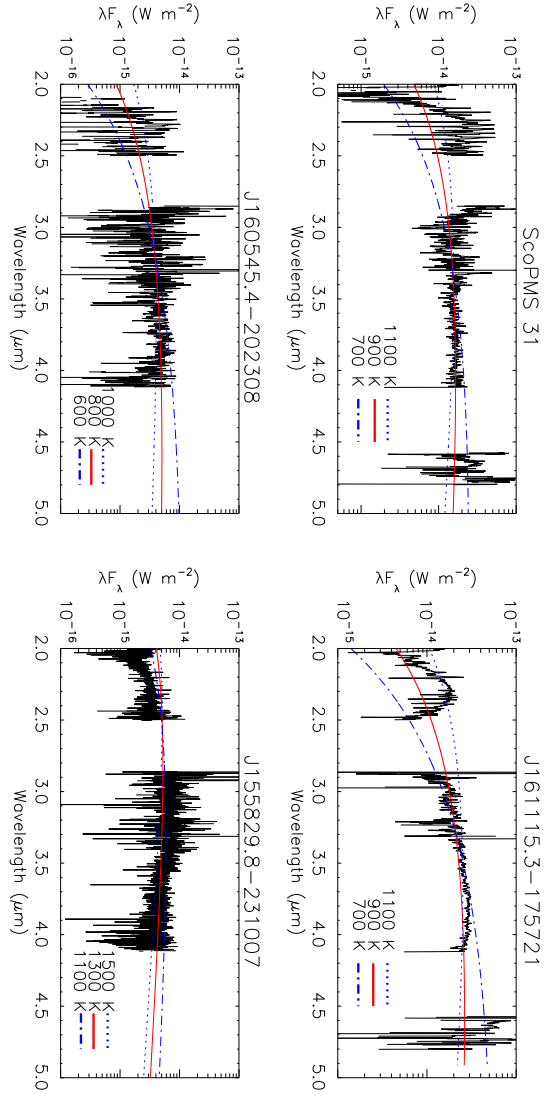


Fig. 3.— (continued)

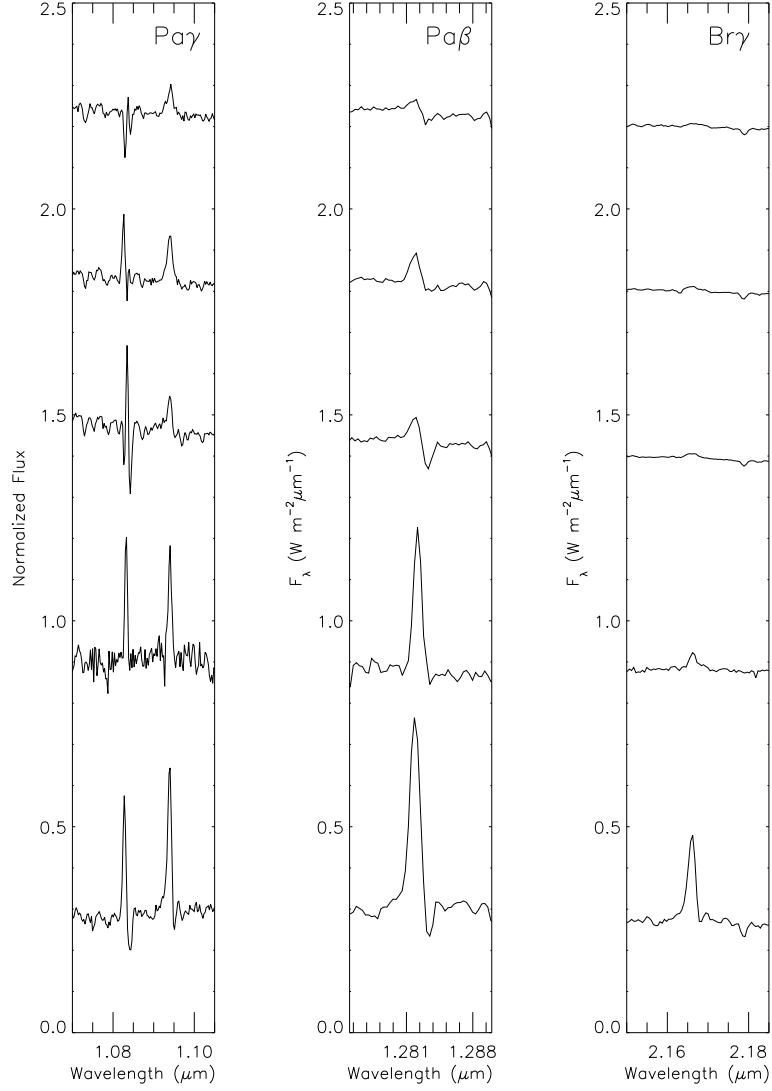


Fig. 4.— Emission features of He I  $\lambda 10830$  and Pa $\gamma$  (left), Pa $\beta$  (center), and Br $\gamma$  (right), for the 5 accreting sources in the sample. From top to bottom, the sources shown are: ScoPMS 31 (M0.5), J160900.7-190852 (K7), [PZ99]J160357.6-203105 (K5), J155829.8-231007 (M3), and J161420.2-190648 (M0).

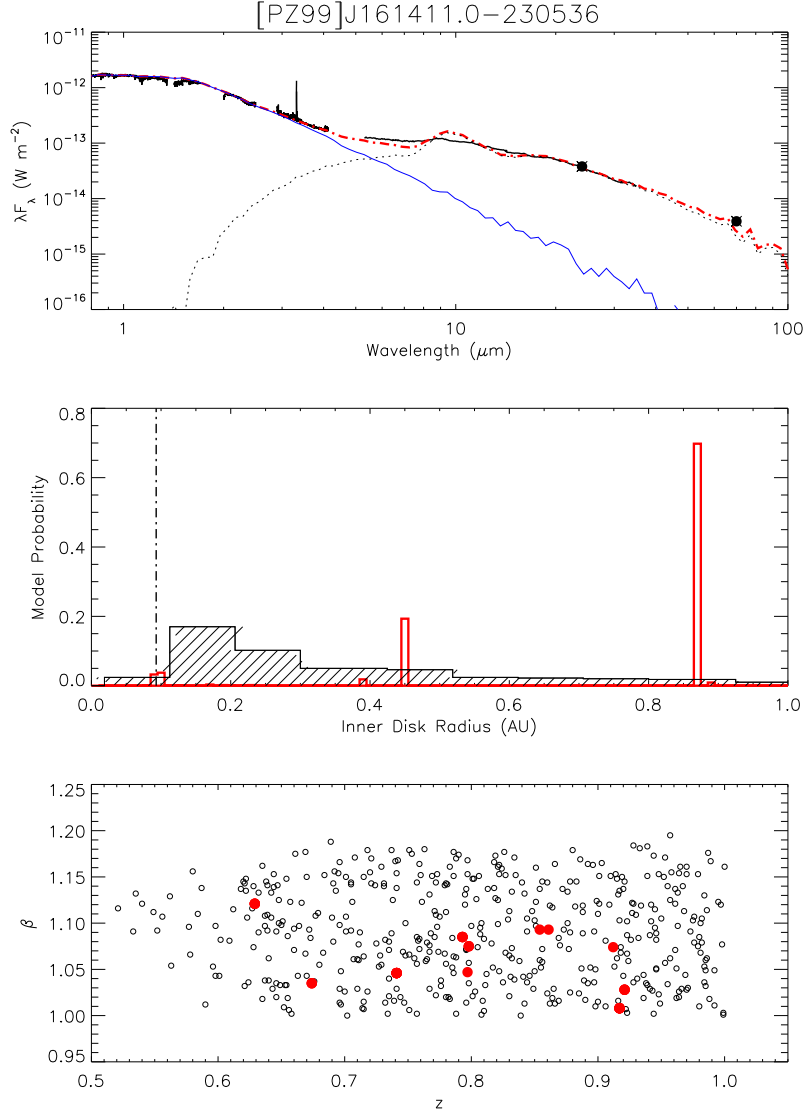


Fig. 5.— (top) The observed 0.8–70.0  $\mu$ m SEDs for 9 late-type Upper Scorpius disk-bearing stars constructed from the SpeX 0.8–5.2  $\mu$ m spectra, the *Spitzer* IRS 5.4–37.0  $\mu$ m spectra, and the MIPS 24 and 70  $\mu$ m photometry. Superimposed in red are the best-fitting model profiles of Robitaille et al. (2006), placed at their respective distances and extinctions. The disk contributions to the model SEDs are shown as dotted black curves, and the model stellar photospheres from the Kurucz (1979) atlas as solid blue curves. (center) The probability ( $P$ ) of inner disk radii ( $R_{in}$ ) for the Upper Scorpius disk-bearing sample plotted as a function  $R_{in}$ . Superimposed in the figures as cross-hatched histograms are the distributions of inner disk radii for the entire sample of models considered for each source. The vertical dashed lines represent the dust sublimation radii for the best-fitting models. (bottom) The disk flaring parameter ( $\beta$ ) plotted as a function of disk scale height factor ( $z$ ) for all models examined in the SED fitting process. The best-fitting models are shown in red.

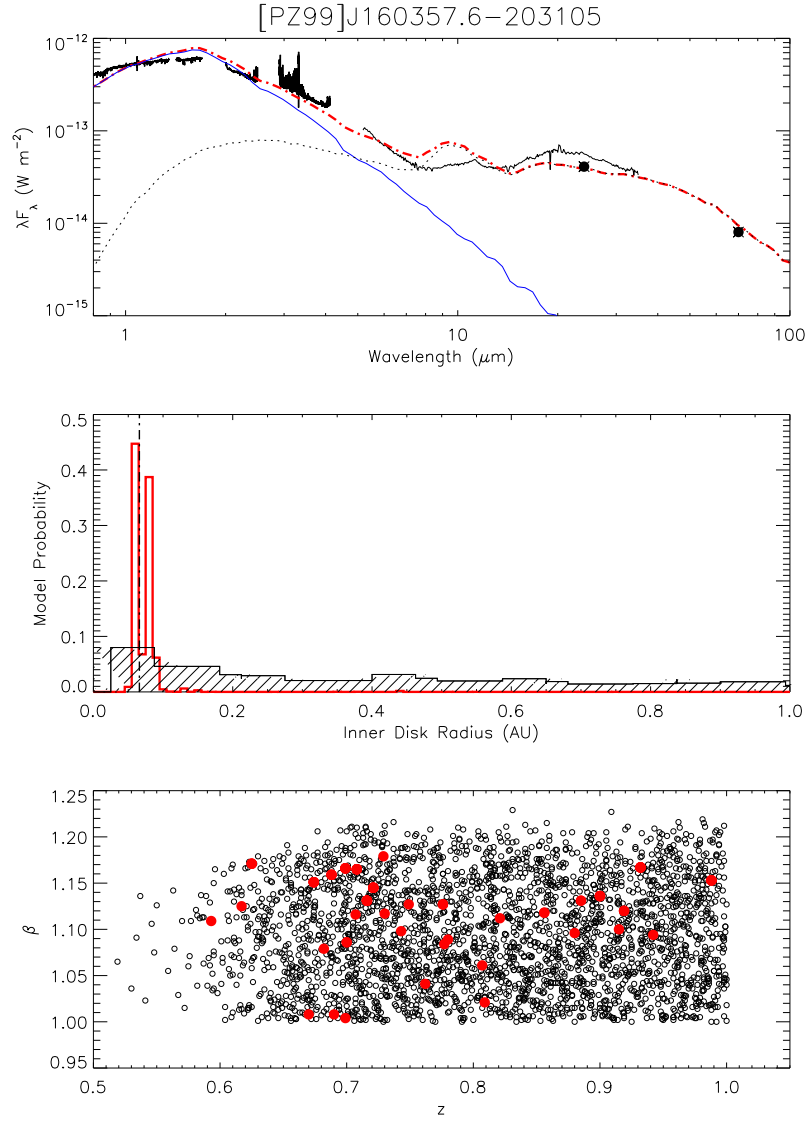


Fig. 5.— (continued)



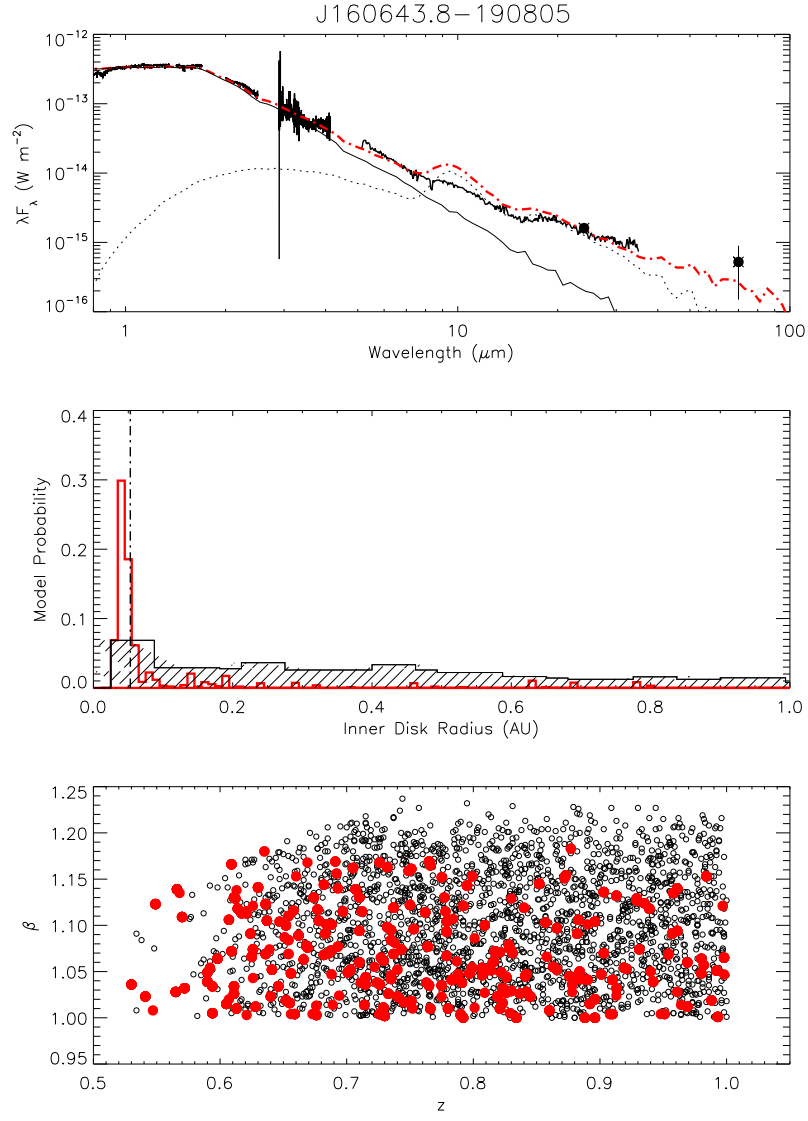


Fig. 5.— (continued)

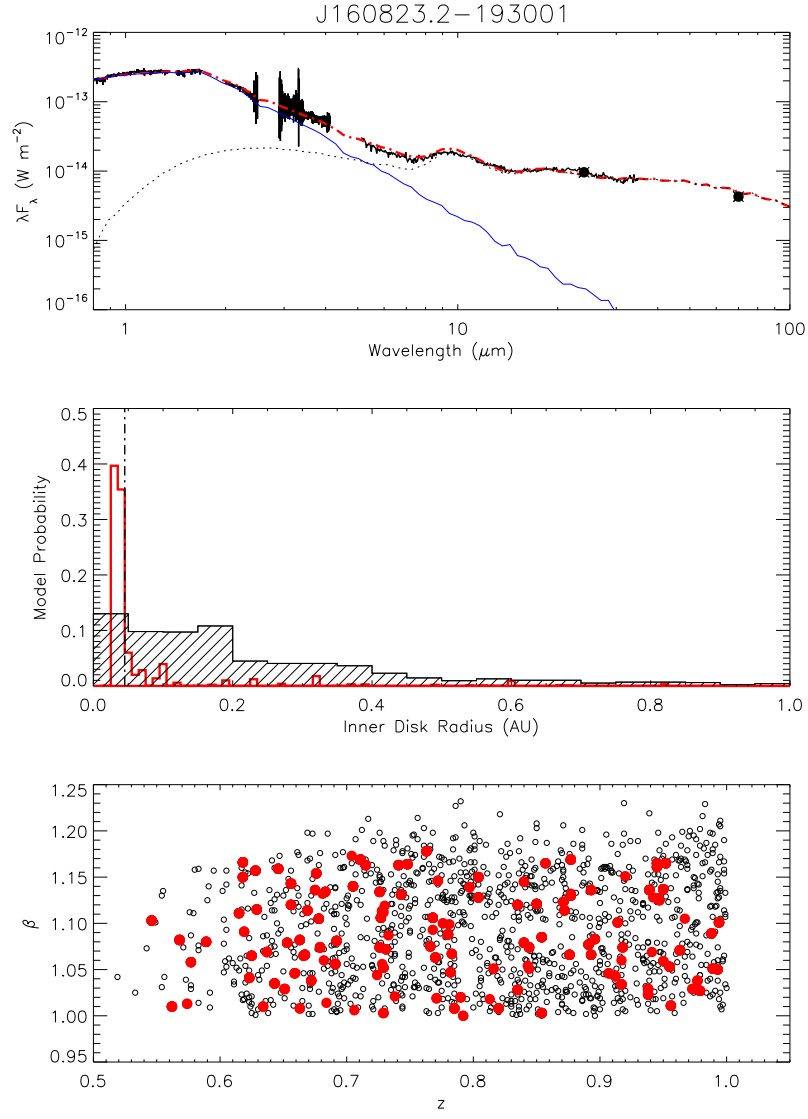


Fig. 5.— (continued)

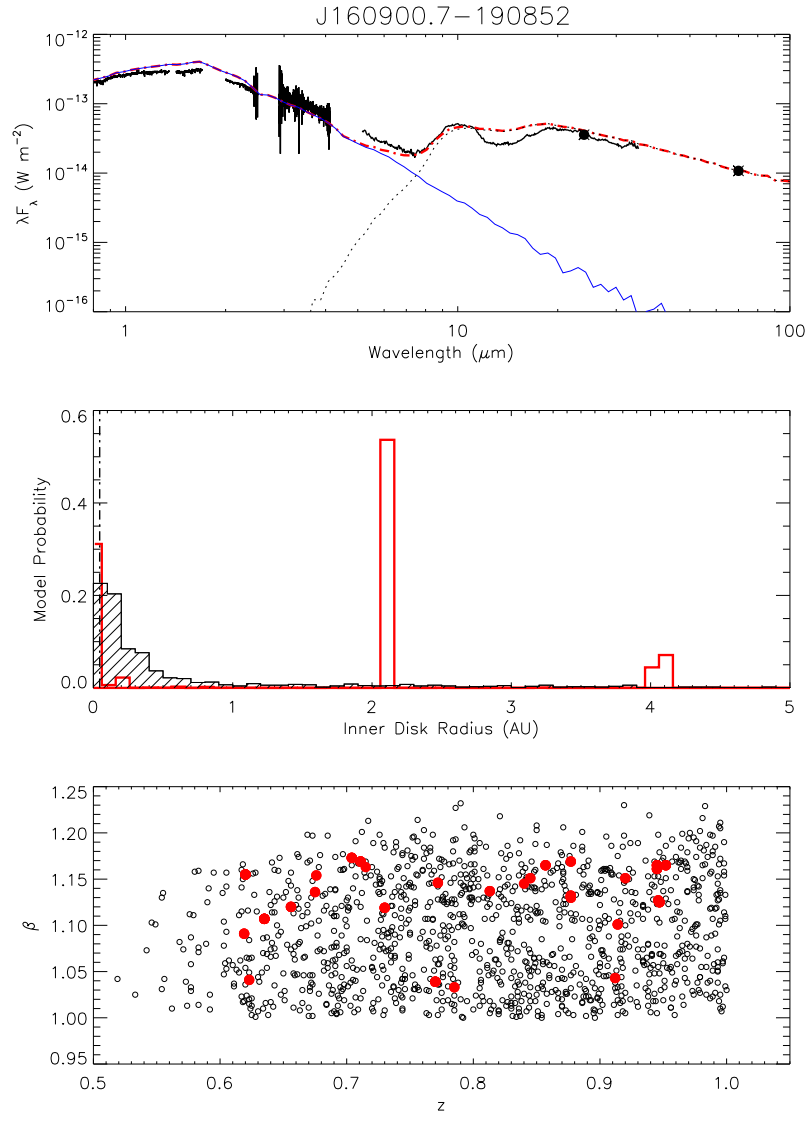


Fig. 5.— (continued)

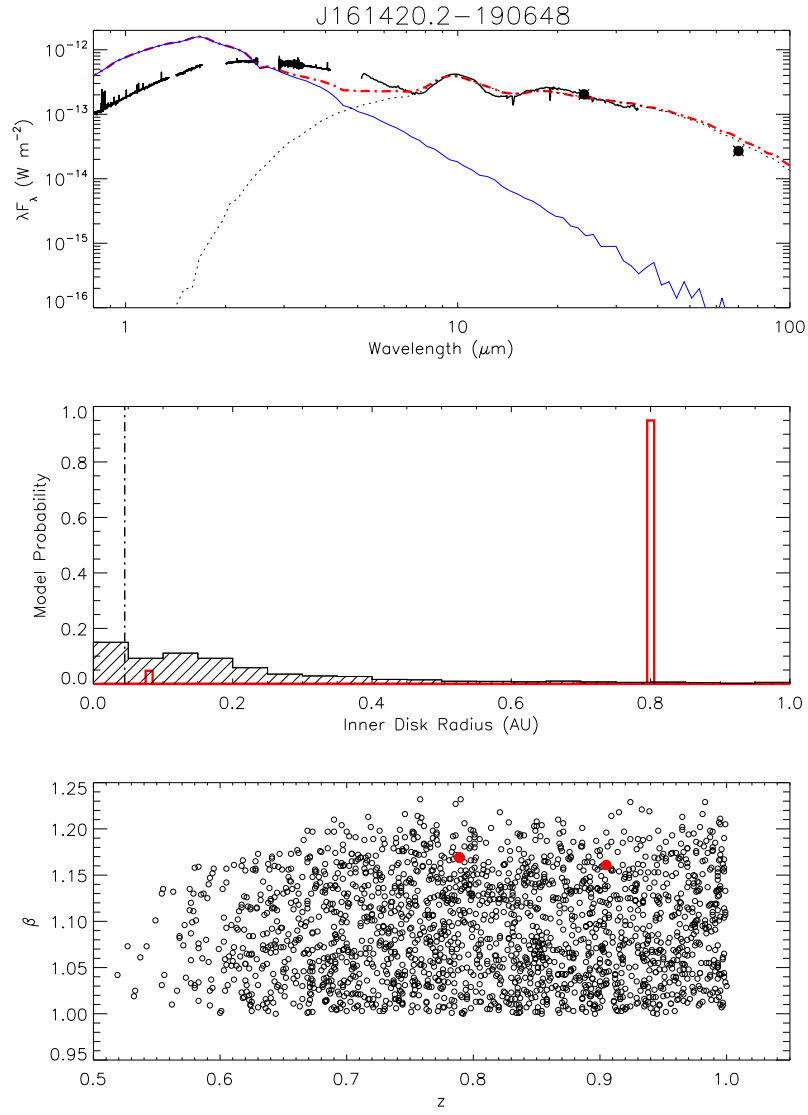


Fig. 5.— (continued)

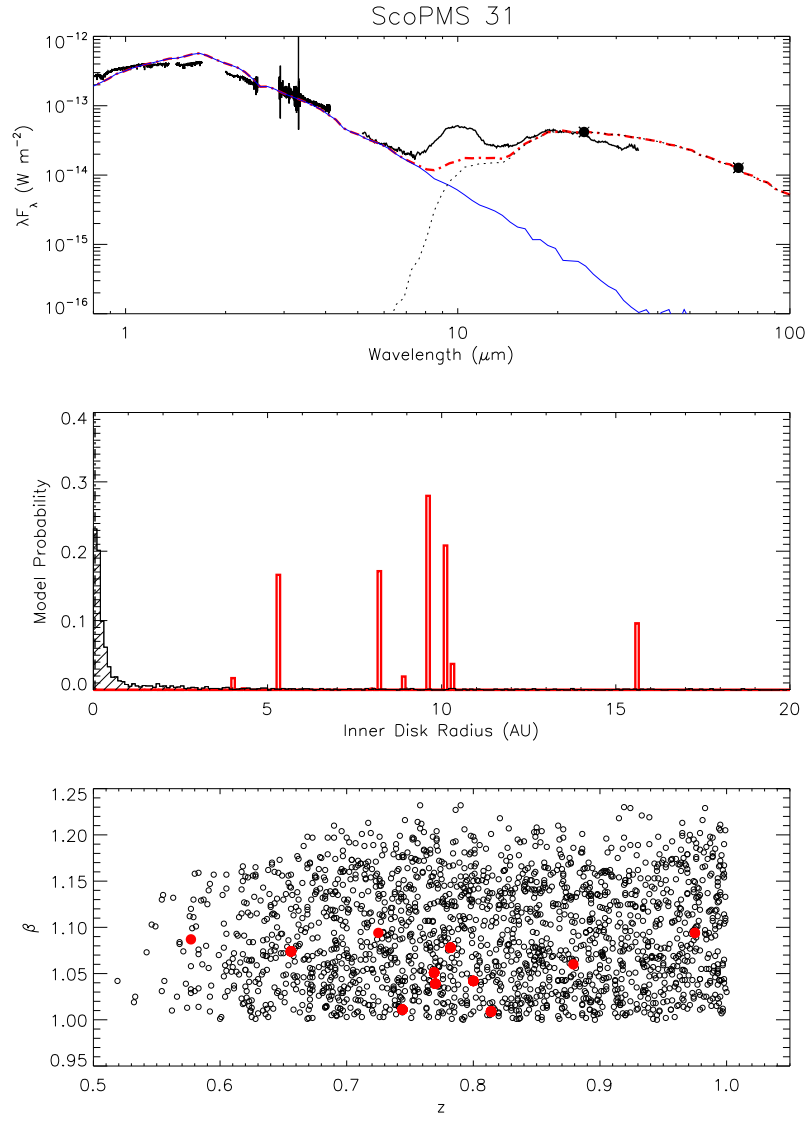


Fig. 5.— (continued)

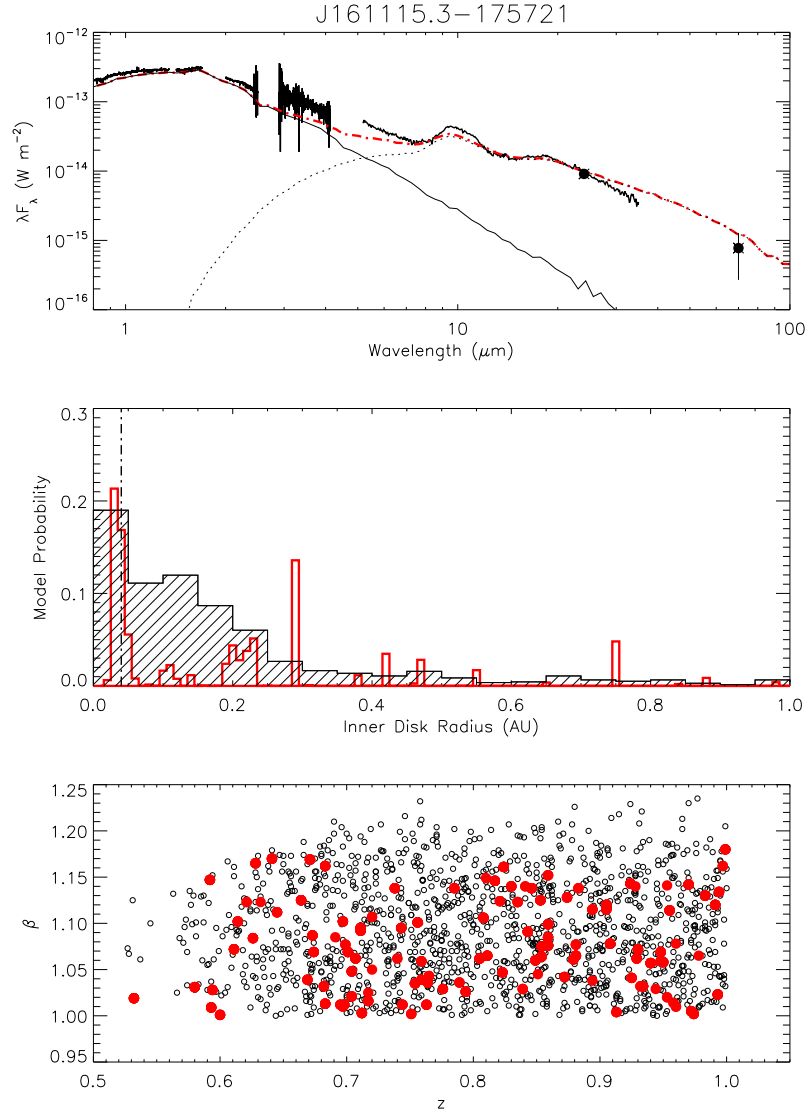


Fig. 5.— (continued)

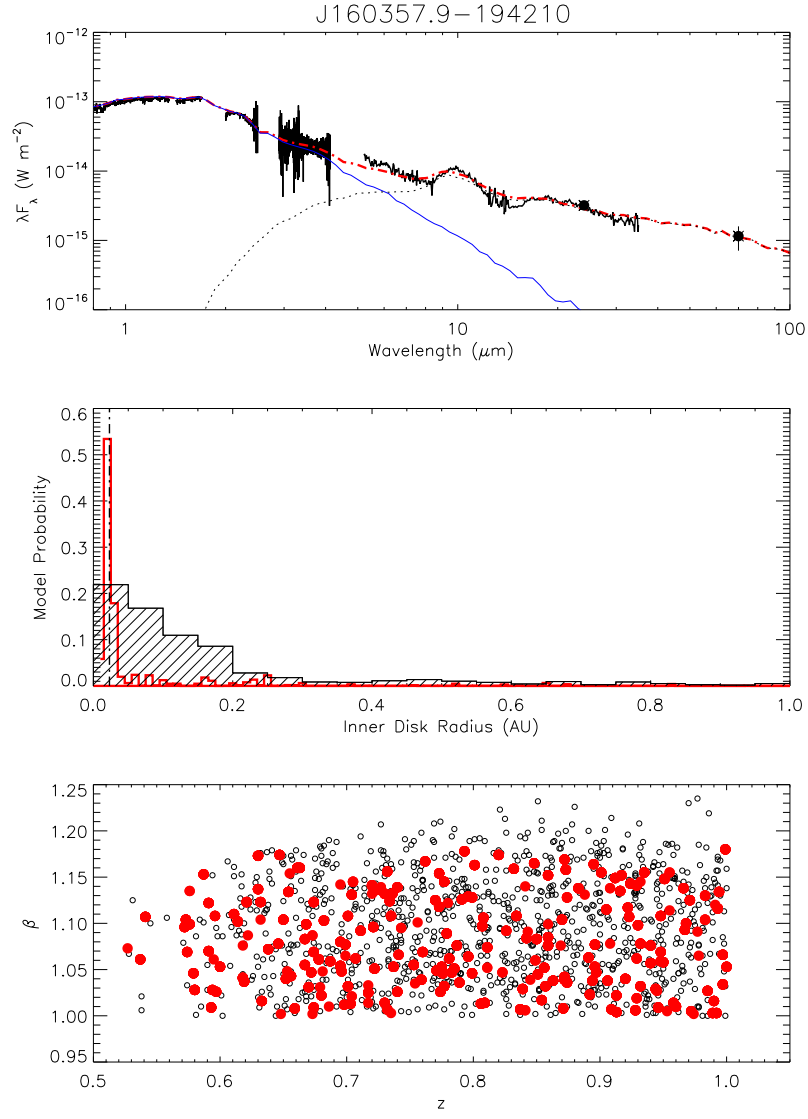


Fig. 5.— (continued)

Table 1. Stellar Characteristics and Excess Properties of the Upper Scorpius Sample

Source <sup>a</sup>	SpT <sup>b</sup>	$A_V$ <sup>c</sup> (mag)	Mass <sup>d</sup> ( $M_\odot$ )	Radius <sup>d</sup> ( $R_\odot$ )	Luminosity <sup>d</sup> ( $L_\odot$ )	$T_{eff}$ <sup>d</sup> (K)	$T_D$ <sup>e</sup> (K)
[PZ99]J161411.0-230536	K0	2.4	1.98	2.65	5.62	5329	700
[PZ99]J160421.7-213028	K2	1.0	1.08	1.14	0.74	4893	900
[PZ99]J160357.6-203105	K5	0.9	1.09	1.59	0.82	4321	1300
J160643.8-190805	K6	1.9	0.95	1.42	0.65	4205	$\leq 500$
J160823.2-193001	K9	1.5	0.70	1.23	0.37	3963	800
J160900.7-190852	K9	0.8	0.69	1.24	0.43	3963	1300
J161420.2-190648	M0	1.8	0.56	1.55	0.52	3840	1300
ScoPMS 31	M0.5	0.9	0.52	1.63	0.60	3782	900
J161115.3-175721	M1	1.6	0.48	1.55	0.48	3725	900
J160357.9-194210	M2	1.7	0.40	1.06	0.17	3611	$\leq 500$
J160545.4-202308	M2	2.2	0.36	1.05	0.16	3530	800
J155829.8-231007	M3	1.3	0.25	0.60	0.05	3380	1300

<sup>a</sup>Identifiers from Carpenter et al. (2006).

<sup>b</sup>Spectral type from the literature.

<sup>c</sup>Extinction estimates are taken from Preibisch & Zinnecker (1999) and Preibisch et al. (2002).

<sup>d</sup>From the models of Siess et al. (2000), assuming a distance of 145 pc.

<sup>e</sup>Dust temperature derived from the blackbody fits of the continuum excess emission.



Table 2. Accretion Luminosities and Derived Mass Accretion Rates

Source	EW(Pa $\beta$ ) <sup>a</sup> (Å)	EW(Br $\gamma$ ) <sup>a</sup> (Å)	$\log L_{acc}(\text{Pa}\beta)/L_{\odot}$ <sup>b</sup>	$\log L_{acc}(\text{Br}\gamma)/L_{\odot}$ <sup>b</sup>	$\log \dot{M}(\text{Pa}\beta)^c$	$\log \dot{M}(\text{Br}\gamma)^c$
[PZ99]J160357.6-203105	−0.51	−0.58:	−2.23±0.18	−2.00±0.23	−9.47±0.18	−9.23±0.27
J160900.7-190852	−1.35	−2.20	−2.04±0.15	−1.74±0.18	−9.19±0.15	−8.89±0.18
J161420.2-190648	−3.40	−3.69	−1.48±0.10	−0.65±0.10	−8.40±0.10	−7.60±0.10
ScoPMS 31	...	−1.45	...	−1.62±0.17	...	−8.52±0.17
J155829.8-231007	−4.15	−3.27	−2.37±0.20	−2.50±0.31	−9.39±0.20	−9.52±0.31

<sup>a</sup>Negative equivalent width implies emission.

<sup>b</sup>Accretion luminosity determined using the linear relationship of Muzerolle et al. (1998).

<sup>c</sup> $\dot{M}$  derived assuming  $R_*$ ,  $T_{eff}$ , and  $M_*$  values listed in Table 1.

Table 3. Accretion Disk Models

Source	$T_{eff}$ Range <sup>a</sup> (K)	Number <sup>b</sup>	Model ID <sup>c</sup>	$A_V$ <sup>d</sup> (mag)	$d$ <sup>d</sup> (pc)	$i$ <sup>d</sup> ( $^\circ$ )	$\chi^2$ <sup>d</sup>
[PZ99]J161411.0-230536	4900–5410	500	3014849	1.0	125	75.5	6.30
[PZ99]J160357.6-203105	4205–4590	2993	3012326	2.0	125	31.8	13.44
J160643.8-190805	4060–4350	2753	3005191	0.5	185	75.5	1.51
J160823.2-193001	4850–4060	1190	3013325	0.75	165	41.4	0.34
J160900.7-190852	4850–4060	1190	3019185	1.0	145	81.4	4.72
J161420.2-190648	3580–4060	1998	3008376	3.0	125	56.6	58.91
ScoPMS 31	3729–4060	1917	3002397	2.0	165	81.4	2.19
J161115.3-175721	3580–3850	1409	3016046	2.0	165	41.4	2.87
J160357.9-194210	3470–3720	1180	3018769	0.5	155	63.3	0.42

<sup>a</sup> $T_{eff}$  range considered for the adopted spectral type of the source.

<sup>b</sup>The number of models having  $T_{eff}$  values within the specified range.

<sup>c</sup>The best-fitting model identification number from Robitaille et al. (2006).

<sup>d</sup>Extinction, distance, inclination angle, and reduced  $\chi^2$  values for the best-fitting model.

Table 4. Inferred Disk Properties of the Upper Scorpius Sources

Source	$M_{disk} (M_{\odot})^a$			$\dot{M} (M_{\odot} \text{ yr}^{-1})^a$			$R_{in} (\text{AU})^a$		
	(min)	(best)	(max)	(min)	(best)	(max)	(min)	(best)	(max)
[PZ99]J161411.0-230536	7.18E-7	1.06E-5	1.16E-2	2.88E-13	2.43E-11	5.13E-8	0.10	0.87	2.24
[PZ99]J160357.6-203105	2.60E-6	2.62E-5	3.47E-2	6.79E-13	1.16E-11	6.97E-8	0.06	0.07	0.14
J160643.8-190805	5.30E-8	3.70E-6	5.34E-3	5.06E-15	2.28E-14	2.22E-9	0.04	0.05	10.00
J160823.2-193001	6.07E-6	4.30E-4	1.72E-2	4.44E-12	2.02E-11	3.25E-8	0.03	0.04	1.19
J160900.7-190852	1.44E-5	6.56E-3	6.56E-3	4.44E-12	1.43E-9	6.05E-9	0.04	2.18	4.13
J161420.2-190648	4.28E-5	4.28E-5	1.36E-3	3.31E-10	3.31E-10	1.17E-7	0.08	0.80	0.80
ScoPMS 31	5.90E-5	8.24E-4	1.45E-3	1.31E-12	3.57E-9	5.20E-9	4.08	9.62	15.70
J161115.3-175721	3.52E-7	3.53E-5	1.78E-2	2.69E-13	1.74E-11	4.10E-8	0.03	0.29	1.19
J160357.9-194210	3.62E-7	2.50E-4	9.50E-3	2.41E-13	2.16E-11	1.63E-8	0.02	0.17	1.29

<sup>a</sup>Minimum, best-fitting, and maximum  $M_{disk}$ ,  $\dot{M}$ , and  $R_{in}$  values of the subset of best-fitting models of Robitaille et al. (2006).